AGU PUBLICATIONS

Geochemistry, Geophysics, Geosystems

RESEARCH ARTICLE
10.1002/2013GC005138

Empirical evidence for the fractionation of carbon isotopes between diamond and iron carbide from the Earth's mantle

S. Mikhail[1,2,3], C. Guillermier[2], I. A. Franchi[2], A. D. Beard[4], K. Crispin[3], A. B. Verchovsky[2], A. P. Jones[1], and H. J. Milledge[1]

[1]Department of Earth Sciences, University College London, London, UK, [2]Department of Physical Sciences, Open University, Milton Keynes, UK, [3]Geophysical Laboratory, Carnegie Institution of Washington, Washington, D. C., Washington, 20015, USA, [4]Department of Earth and Planetary Sciences, Birkbeck, College University of London, London, UK

Key Points:
- In the mantle, C isotope fractionation may be larger in the hotter deep mantle
- Carbide precipitation can produce isotopically distinct mantle carbon reservoirs
- Core formation likely fractionated the C isotope value of the BSE

Supporting Information:
- Read Me
- Figure S1, S2, S3, S4

Correspondence to:
S. Mikhail,
smikhail@ciw.edu

Citation:
Mikhail, S., C. Guillermier, I. A. Franchi, A. D. Beard, K. Crispin, A. B. Verchovsky, A. P. Jones, and H. J. Milledge (2014), Empirical evidence for the fractionation of carbon isotopes between diamond and iron carbide from the Earth's mantle, *Geochem. Geophys. Geosyst.*, *15*, 855–866, doi:10.1002/2013GC005138.

Received 6 NOV 2013
Accepted 1 JAN 2014
Accepted article online 8 JAN 2014
Published online 2 APR 2014

Abstract We have studied two samples of mantle diamond containing iron carbide inclusions from Jagersfontein kimberlite, South Africa. Syngenetic crystal growth is inferred using morphological characteristics. These samples provide an opportunity to investigate the isotopic partitioning of ^{13}C in a terrestrial natural high-pressure and high-temperature (HPHT) system. The difference for the $\delta^{13}C$ values between the diamond and coexisting iron carbide averaged $7.2 \pm 1.3‰$. These data are consistent with available data from the literature showing iron carbide to be ^{13}C-depleted relative to elemental carbon (i.e., diamond). We infer that the minerals formed by crystallization of diamond and iron carbide at HPHT in the mantle beneath the Kaapvaal Craton. It is unclear whether crystallization occurred in subcratonic or sublithospheric mantle; in addition, the source of the iron is also enigmatic. Nonetheless, textural coherence between diamond and iron carbide resulted in isotopic partitioning of ^{13}C between these two phases. These data suggest that significant isotopic fractionation of $^{13}C/^{12}C$ ($\Delta^{13}C$ up to $>7‰$) can occur at HPHT in the terrestrial diamond stability field. We note that under reducing conditions at or below the iron-iron wustite redox buffer in a cratonic or deep mantle environment in Earth, the cogenesis of carbide and diamond may produce reservoirs of ^{13}C-depleted carbon that have conventionally been interpreted as crustal in origin. Finally, the large $\Delta^{13}C$ for diamond-iron carbide shown here demonstrates $\Delta^{13}C$ for silicate-metallic melts is a parameter that needs to be constrained to better determine the abundance of carbon within the Earth's metallic core.

1. Introduction

The stable isotopes of carbon from mantle-derived samples are frequently used to trace the exchanges of carbon between the Earth's surface and interior. Relevant examples include the degassing history of subducted slabs using volcanic gas compositions at convergent plate boundaries (see review by *Wallace* [2005]) and the origin of diamond-forming carbon (see review by *Shirey et al*. [2013]). Regarding the use of carbon isotopes as source indicators, there are three main parameters that need to be constrained before the data can be interpreted with confidence. These are (i) the initial $^{13}C/^{12}C$ ratio in the system, (ii) a database to relatively evaluate the data, and (iii) the magnitude and directions of isotopic fractionation under the P-T-fO_2 conditions in question. These three criteria are mostly well satisfied with regard to the stable isotopes of carbon in the Earth under redox conditions around the quartz-fayalite-magnetite (QFM) buffer (see *Deines* [2002] for a review). However, carbon isotope fractionation in the mantle around the Fe-FeO (IW) buffer ($\approx$ QFM -4 log units) is considerably less well constrained. In this paper, we focus on the partitioning of $^{13}C/^{12}C$ during diamond formation under conditions where metallic iron and iron carbides are thermodynamically stable (log $fO_2 <$ IW buffer), using two very rare samples of Fe-carbide bearing diamond (Figure 1).

The magnitudes of isotopic fractionation during diamond formation in the mantle buffered around QFM at 1200°C are $+1‰$ for diamond-CH_4 [*Bottinga*, 1969; *Thomassot et al*., 2007] and $-3.5‰$ for diamond-CO_2 [*Richet et al*., 1977]. When the fO_2 is buffered below the IW buffer, much larger $\Delta^{13}C$ values have been observed (where $\Delta^{13}C = (1000)*\ln\alpha \approx \delta^{13}C_{phase\ 2} - \delta^{13}C_{phase\ 2}$ in parts per mil). In iron meteorites, the reaction graphite-Fe carbide shows a $\Delta^{13}C$ of $+12‰$ for an unknown temperature, where the carbide is ^{13}C-depleted

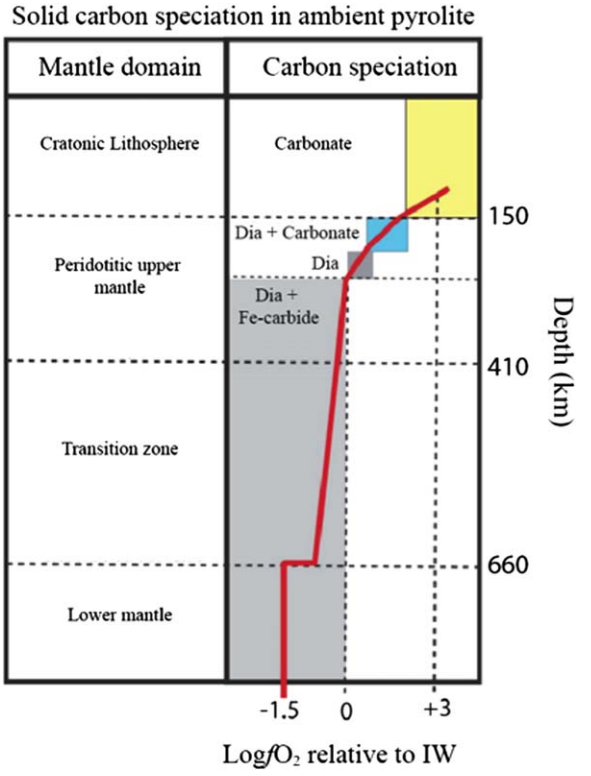

Figure 1. The speciation of solid carbon as a function of the fO_2 with depth in an ambient pyrolitic mantle (modified from *Rohrbach and Schmidt* [2011]). Note the dominance in the bulk terrestrial mantle of reduced (carbide) and neutral (diamond) carbon species relative to oxidized carbon (carbonate). The base of cratonic lithosphere positioned at 150 km relates to the average depth of the continental cratonic keels [*Shirey et al*., 2013].

[*Deines and Wickman*, 1975] a phenomenon recently demonstrated experimentally. *Satish-Kumar et al*. [2011] (assumed equilibrium) and *Reutsky et al*. [2012] (kinetic isotope effect) have confirmed that Fe-carbide melts should show ^{13}C-depletion relative to graphite and diamond, but whether or not the experimental data in *Satish-Kumar et al*. [2011] reached isotopic equilibrium is debatable (see the comment by *Reutsky and Borzdov* [2013] and reply by *Satish-Kumar et al*. [2013]). There are also data for Si-carbides; these show an even larger $\Delta^{13}C$ of around $+20‰$ for moissanite-diamond [*Leung et al*., 1990; *Mathez et al*., 1995] and $\Delta^{13}C$ of around $16‰$ for carbonate-Si carbide [*Di Pierro et al*., 2003], the latter most likely a kinetic effect. Most of these studies used conventional oxidation techniques at high temperature to oxidize the carbon to CO_2 for analysis from mineral separates [*Leung et al*., 1990; *Mathez et al*., 1995; *Di Pierro et al*., 2003; *Reutsky et al*., 2012; *Satish-Kumar et al*., 2011]. Therefore the data are bulk values and reflect the contents in the furnace at the moment of oxidation. Noteworthy, the isotopic compositions of the phases determined by bulk combustion methods can be skewed by the presence of one phase contaminating the other, especially for very small pieces of graphite/diamond contaminating the carbide analysis (i.e., submicron inclusions/intergrowths).

In this contribution, we describe the textural relations and the major element geochemistry of two diamonds that contain rare Fe-carbide inclusions from Jagersfontein, South Africa (Kaapvaal Craton). We also detail the analytical technique and standardization methods employed to analyze the $^{13}C/^{12}C$ ratio for both diamond and Fe-carbide (in situ) with a spatial resolution of $\approx 5\ \mu m^2$ (per analysis) accomplished using Secondary Ion Mass Spectrometry (NanoSIMS).

2. Samples

There are two samples in this study from the Jagersfontein kimberlite, Kaapvaal Craton, SA [*Jones et al*., 2008]. They are fragmented octahedral diamond and show prominent dark metallic inclusions within opaque diamond directly in contact with surrounding transparent diamond and contain angular shard-like macroscopic features (Figure 2). The samples are polished on both sides to reveal the inclusions at the surface and due to the contrast in sample hardness; some of the carbides have been removed during polishing, leaving depressions. The samples in this study lack nitrogen absorption bands in infrared (IR) spectra and are classified Type II. We have no syngenetic silicate inclusions to demonstrate a paragenesis for these samples and also their host rock is unknown as they were received as loose diamonds (not "in situ"). Therefore, we cannot assign a paragenesis to these samples, nor an independent depth of origin. These parameters cannot be inferred based on their origin being from Jagersfontein, SA because diamond samples from this kimberlite are different paragenesis and have sampled the mantle across a very wide depth range,

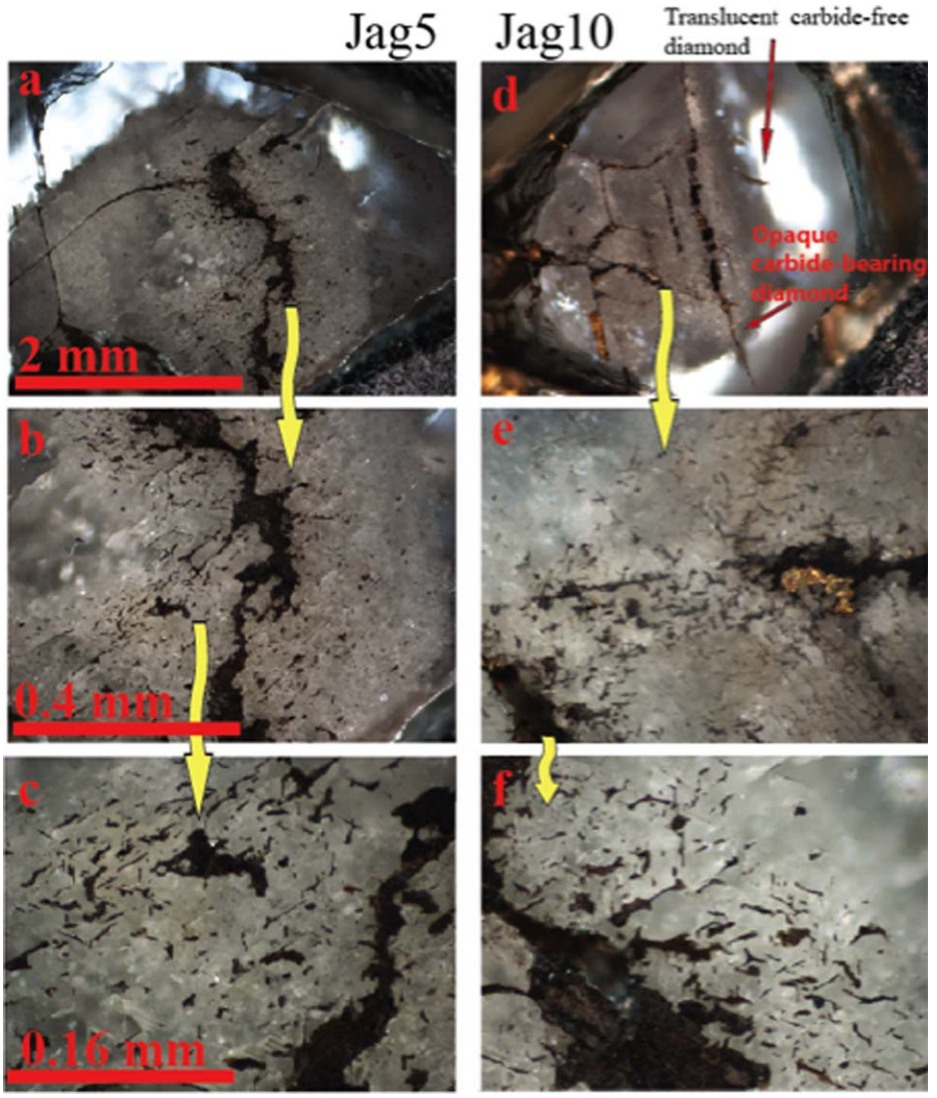

Figure 2. Photomicrographs of the Jagersfontein diamonds with metallic carbide inclusions in both transmitted and reflected light (simultanously). Note the transparency of the Fe-carbide-free sections of the diamonds relative to the diamond surrounding the Fe-carbide and the complexity of the contact textures with increasing magnification.

from approximately 150 to >500 km [*Tappert et al*., 2005]. The Fe-carbide is in contact with diamond as angular shard-like features on the macroscale (Figures 2 and 3b–3d). However, on a microscale the textures exhibit apparent smooth contacts, rounded edges, and possible spherical blebs (Figures 4a–4d) while some inclusions also have a distinctively octahedral morphology (Figures 5a–5c).

3. Analytical Techniques

3.1. EMPA Analysis

Major element analyses were obtained using a JEOL JXA8100 Superprobe (wavelength dispersive spectrometer (WDS)) with an Oxford Instruments INCA system (EDS) at Birkbeck College, University of London (UK). Analysis was carried out using an accelerating voltage of 15 kV, a beam current of 2.5 μA with a diameter of 5 μm. The counting times for the elements were 20 s on the peak and 10 s each on the high and low backgrounds. The elements were calibrated against natural standards of corundum (Al and O) and pyrite (S), Specpure® metals (Si, Fe, Cr, Ni, Cr, and CO), and synthetic moissanite (C) with the data corrected using a ZAF program. To prevent volatilization and electron-induced migration of carbon, a shorter counting time of 10 s on the carbon peak and 5 s each on the high and low backgrounds was employed.

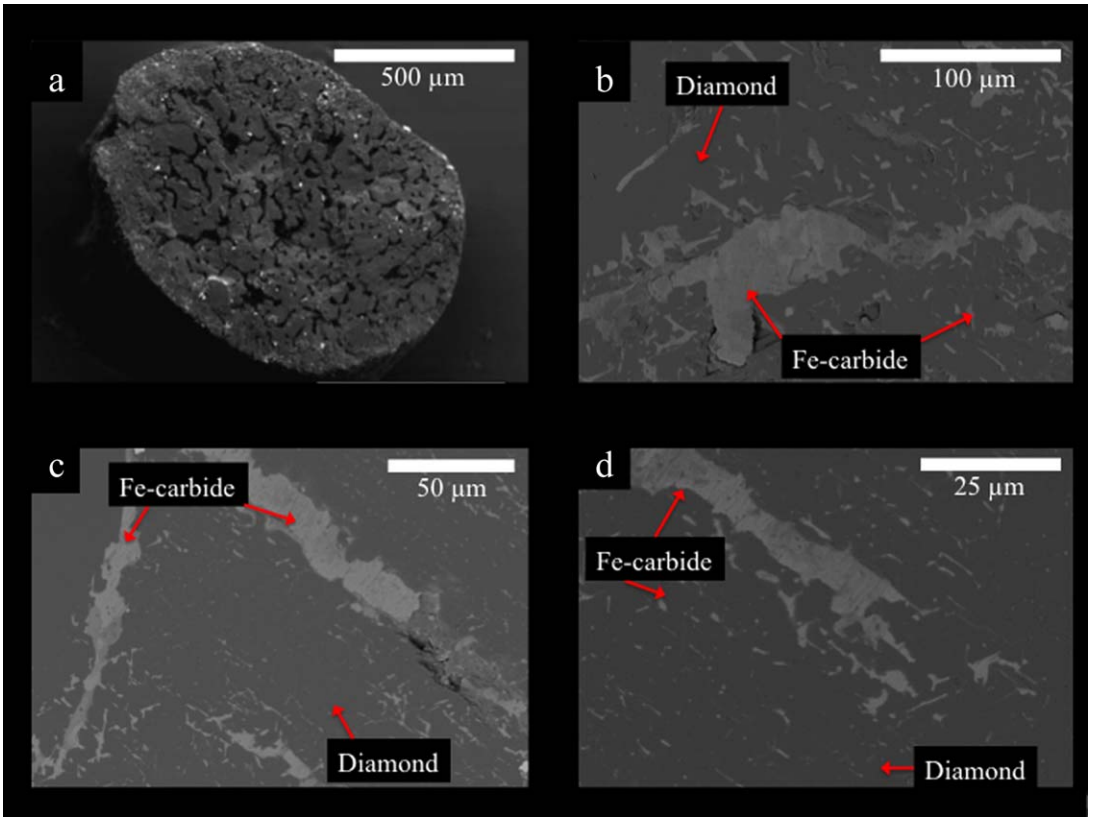

Figure 3. SEM images demonstrating textural relationships between the Fe-carbide and the diamond host. The slight colouration discrepancies in the Fe-carbide proportions relate to topographic features as a function of the polishing procedure. (a) SAMPLE S3636 from *Tomlinson et al.* [2011] synthesised at 20 GPa, 2100°C. This is a capsule slice with solvent catalyst is removed to show "brain-like" texture of amalgamated diamond mass present from a diamond grown in a Fe-Ni solvent catalyst. EDS images of textures seen in sample (b and c) Jag5 and (d) in Jag10.

3.2. FE-SEM Analysis

Prior to analysis by nanoSIMS and field-emission scanning electron microscope (FE-SEM), the carbon coat was removed by polishing the sample with a diamond paste and then cleaned in an ultrasonic bath of with ethanol for 10 min. Samples were then pressed in indium for nanosims50L analysis and sputter coated with a 40 nm thick layer of Au (99.99% purity) to enable electrical charge dissipation during the SIMS analysis from the insulating sample to the indium in which it is pressed. Electron dispersive images were produced using a JEOL JSM-6500F: FE-SEM equipped with an Oxford X-Max 80 mm^2 large-area silicon drift detector energy dispersive spectrometer (SDD-EDS) system, in the Carnegie Institution of Washington (USA), and images were generated using an accelerating voltage of 15 kV.

3.3. NanoSIMS Analysis

The $^{13}C/^{12}C$ ratios were determined using a Cameca NanoSIMS 50L ion microprobe in the department of Physical Sciences, The Open University, Milton Keynes (UK). This instrument is equipped with seven detectors (one Faraday cup (FC) and six electron multipliers (EM). The vacuum in the analysis chamber is typically in a 2–5.10^{-10} torr. Quantitative carbon isotope analyses and qualitative elemental imaging were performed using a 16 keV energy Cs+ primary beam of current 15 and 5 pA, respectively. The $^{12}C^-$, $^{13}C^-$, and FeC^- ions were collected in a Faraday cup and two Electron multipliers, respectively. Additional ions-like O^-CN^- and Si were also recorded in EM when assessing potential matrix effects on the precision of the isotopic ratio measurements. For $^{13}C/^{12}C$ ratio determinations, the instrument was tuned at a mass-resolving power of 7000 (Cameca design limit for the 50L nanoSIMS). The current corresponding to the ^{12}C signal during the acquisition was in a 0.3–0.5 pA range as measured in the FC. The corresponding signal in the EM for ^{13}C is in a 20,000–40,000 ct/s range, conditions where the ageing of the detector within a period of 24 h or more is negligible. The EM detector gain and threshold were monitored and corrected if necessary

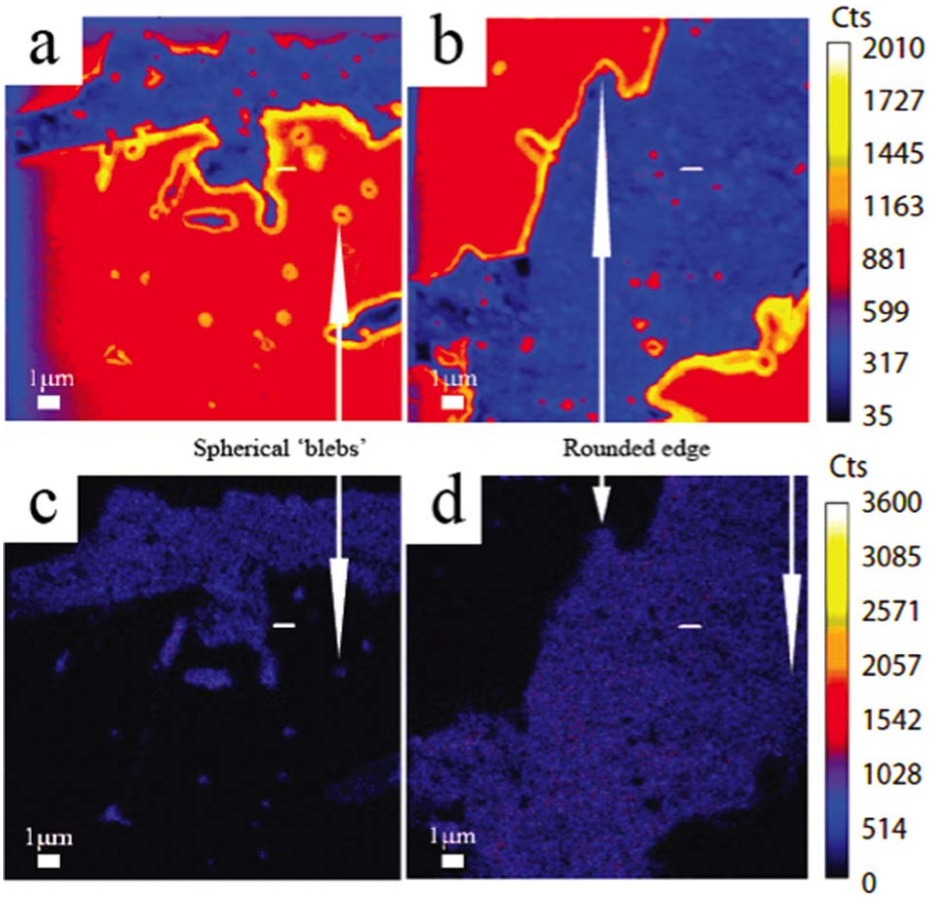

Figure 4. Secondary ion intensity maps from sample Jag5. (a and b) ^{12}C intensity where the red-orange material is diamond and blue is Fe-carbide. (c and d) The coupled $^{12}C^{56}Fe$ intensities where the black area is diamond and the blue is Fe-carbide. Note the small (<0.5 μm^2) spherical "bleb" looking features of Fe-carbide within the diamond host and the "rounded" contact edges between diamond and Fe-carbide.

daily. The EM/FC instrumental drift was controlled by systematically sandwiching the analytical sequence of the unknown (sample) between standards. The size of the analyzed spots was 5 μm^2.

The $^{13}C/^{12}C$ ratios for the standards were obtained from the analyses of independent spots spaced 50 μm apart. Each spot consists in the rapid scanning, 540 ms, of a 5 μm by 5 μm area with a Cs^+ probe of 15 pA. Presputtering for 10 min with a 25 pA Cs beam of the area analyzed prior to acquisition was systematically performed; this procedure ensured removal of any remnant surface contamination or residual carbon coating from the Electron Probe Microanalyzer (EMPA) analysis both for samples and standards. The $^{13}C/^{12}C$ ratio from a spot is the average value of a set of 10 blocks of 50 measurements, e.g., 50 scans, per block. The total analysis time is then 4.5 min per spot, and the counting time is the same for ^{12}C and ^{13}C. The internal error for each spot is the standard deviation of the mean on these 10 blocks and was equal to or better than 1 per mil for most of the standards used. Finally, each single value for the standards reported in this paper is the mean of the $^{13}C/^{12}C$ ratios calculated from a sampling of four spots. The uncertainties reported are the standard deviation and are 1σ for Fe-carbide data and 2σ for diamond data.

Instrumental mass fractionation was corrected using the analyses of standard materials that were loaded in the same sample holder within the same indium metal and analyzed on the same day before and after sample analysis. Standards were cohenite from basaltic rocks sourced from Disko Island, Greenland for cohenite with $\delta^{13}C$ value $= -23.5‰$, a large polished plate of homogeneous laser-sectioned diamond sourced from Drukkers diamond with $\delta^{13}C = -6.0‰$; and synthetic diamond produced by chemical vapor deposition (CVD) with $\delta^{13}C = -62.4‰$. The $\delta^{13}C$ values of the standards and their derived errors (<0.05‰) were determined using an elemental analyzer attached to a Thermo MAT 253 at the Department of

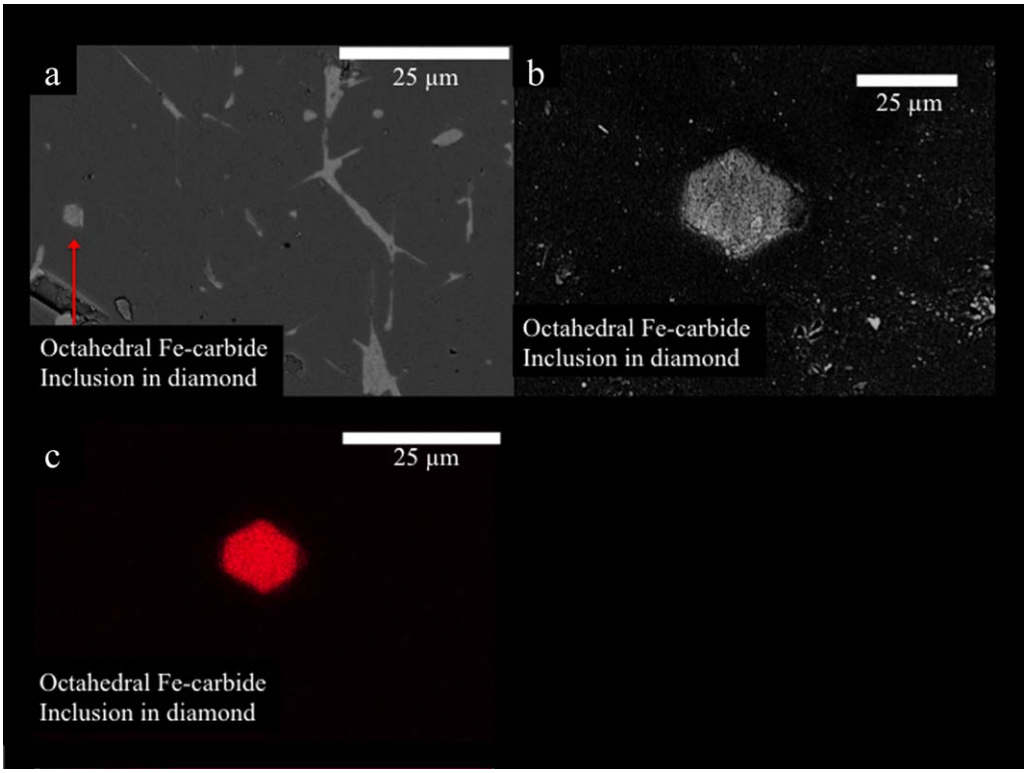

Figure 5. Examples of octahedral Fe-carbide inclusions and a cast observed in samples Jag 5. (a) An examples of an octahedral Fe-carbide grains within the diamond host whilst also showing irregular rounded and sharp Fe-carbide grains within a 50 μm range, (b) a close up of an octahedral Fe-carbide grain in secondary electron imagry, and (c) the same grain as shown in Figure 5b but this image shows the Fe concnetration of the field of view.

Physical Science, The Open University, Milton Keynes (UK). The precision on the standards measured using the nanoSIMS was better than $\pm 1.0‰$ for Disko cohenite, $\pm 2.0‰$ for Drukkers diamond, and $\pm 0.6‰$ for a sample of diamond produced by CVD (Table 1).

The Fe-carbide standard was natural cohenite ($Fe[Ni]_3C$), and the sample which is a previously undescribed Fe-carbide with minor to significant Si and O concentrations, but both the samples and the standard share similar Ni concentrations (Table 2). We used these samples to test for matrix effects for Si and O on the obtained carbon isotope compositions. This was critically evaluated in six sputter pits in Jag10, and achieved by producing elemental maps using the secondary ions generated to detect ^{16}O, ^{28}Si, and $^{14}N^{12}C$ and plotting them against $^{13}C/^{12}C$ ratios. The lack of any correlations between the intensities of ^{16}O, ^{28}Si, and $^{14}N^{12}C$ versus $^{13}C/^{12}C$ ratios for the samples, or standard, lead us to conclude there is no effect of their concentration on the presented $\delta^{13}C$ values (see [1]supporting information Figures S1–S3). These intensities are not quantitative because a suitable Fe-carbide standard with homogeneous O, Si, and N abundances necessary to normalize actual atomic abundances of these elements was unavailable. Therefore, the relative secondary ion counts do not reflect actual atomic ratios because the sputtered secondary ions may have different ionization efficiencies. For imaging, all ions were collected using Electron multipliers.

The precision for our $\delta^{13}C$ determinations range from ± 0.6 to $2.0‰$ (Table 3) and is comparable to a recent study of $\delta^{13}C$ values with a resolution of 4 μm^2 ($\pm 1.9‰$ 2σ) for samples of terrestrial graphite inclusions in silicates from a facility with the same Cameca nanoSIMS 50L specification as this study [see *Papineau et al.*, 2010].

4. Results

The major element geochemistry of the carbides is shown in Table 2. The two samples analyzed contain from 88 to 90 wt % Fe. This is similar in composition to rare terrestrial carbide in garnet inclusions from

Table 1. Data for the Standards[a]

Cohenite	$\delta^{13}C_{PDB}$	Mean$\delta^{13}C_{PDB}$	Precision (‰)
DISKO-A-1	−24.71	−24.92	0.38
DISKO-A-2	−25.36		
DISKO-A-3	−24.71		
DISKO-B-1	−20.96	−22.07	0.79
DISKO-B-2	−22.07		
DISKO-B-3	−22.73		
DISKO-B-4	−22.54		
DISKO-C-1	−22.76	−23.04	0.33
DISKO-C-2	−23.41		
DISKO-C-3	−22.94		
DISKO-D-1	−23.87	−23.94	0.48
DISKO-D-2	−24.15		
DISKO-D-3	−23.31		
DISKO-D-4	−24.43		
Diamond	$\delta^{13}C_{PDB}$	Mean$\delta^{13}C_{PDB}$	± (‰)
DRUKER-A-1	−4.95	−5.88	1.54
DRUKER-A-2	−5.04		
DRUKER-A-3	−7.65		
DRUKER-B1	−7.23	−6.12	1.08
DRUKER-B-2	−6.06		
DRUKER-B-3	−5.07		
CVD-A-1	−62.6	−62.33	0.42
CVD-A-2	−62.51		
CVD-A-3	−61.87		
CVD-A-4	−62.6		
CVD-A-5	−63.05		

[a]The equations and methods for counting statistics used to calculate the permil standard errors and $\delta^{13}C$ values were sourced from *Fitzsimons et al.* [2000]. The $\delta^{13}C$ value for the standards was acquired using a elemental analyzer attached to a Thermo MAT 253 at the Open University. The $\delta^{13}C$ values are as follows: Disko cohenite is −23.5‰; the diamonds were −6‰ for Drukker and −62.5‰ for CVD. The associated errors on these determinations were better than ±0.05‰.

polycrystalline diamonds from the Venetia kimberlite (Table 2; see section 5.). Overall, the concentrations for Cr, Si, and O vary considerably between the two samples investigated. Noteworthy, the Ni, S, and Co concentrations are low, as is the case for Fe-carbide from Disko Island, Greenland (selected as an isotopic standard for NanoSIMS analysis; Table 1).

The data for the isotopic values obtained are shown in Table 3. The equations and methods for counting statistics used to calculate per mil standard error and $\delta^{13}C$ values were sourced from *Fitzsimons et al.* [2000]. The $\delta^{13}C$ values for the individual diamonds differ where Jag5 has a mean value of -12.7 ± 1.6‰ and Jag10 has a mean value of -17.3 ± 0.6‰. Both values fall into the low-$\delta^{13}C$ group observed for diamonds from Jagersfontein [*Deines et al.*, 1991; *Boyd and Pillinger*, 1994]. The $\delta^{13}C$ values for the individual Fe-carbides also differ where Jag5 has a mean value of -18.6 ± 1.14‰ and Jag10 has a mean value of -25.2 ± 2.1‰. Irrespective of the differences for the mean diamond $\delta^{13}C$ values, the values for $\Delta C_{C\text{-}FeC}$ are comparable (Table 3). The overall mean $\Delta C_{C\text{-}FeC}$ for both samples is $+7.2 \pm 1.3$‰. The $\Delta C_{C\text{-}FeC}$ is expressed using the following equations;

1. $\alpha = (\delta^{13}C_{phase\ 1} + 1000)/(\delta^{13}C_{phase\ 2} + 1000)$

2. $\Delta C_{C\text{-}FeC}$ is defined as $\Delta C = (1000)^{*}\ln\alpha \approx \delta^{13}C_{phase\ 2} - \delta^{13}C_{phase\ 2}$ in parts per mil (‰)

5. Discussion

5.1. Syngenetic or Epigenetic?

Prior to a discussion for the isotopic data first we discuss evidence for syngenesis between the diamond and Fe-carbide. During the review process, the possibility was raised that the Fe-carbide may be a veneer

Table 2. Elemental Concentrations of Various Carbides[a]

	Jag5	Jag10	Venetia	Cohenite	Cementite	Disko Cohenite
Fe	88.42	90.28	90.41	54.92	94.73	92.03
Cr	2.04	0.02				
Ni	0.33	0.10	1.61	28.86		0.66
Co	0.21	0.18	0.37	9.66		
Si	1.65	0.78	0.03			
S	0.02	0.07	0.21			
O	0.97	3.99				
C	5.86	4.51	6.53	6.56	5.27	6.79
Total	99.44	100.00	100.00	100.00	100.00	99.48
Atomic Fe/C	3.25	4.31	2.98	1.80	3.87	2.91

[a]There are two analyses from Jagersfontein carbides labelled Jag5 and Jag10. Data for Disko cohenite is from the RRUFF database [*Downs*, 2006], and cementite data are theoretical compositions calculated assuming an ideal stoichiometric balance. Data for Fe-Ni carbide microspherules in garnet inclusions from Venetia diamond are from *Jacob et al.* [2004] and the data for Disko carbide is from *Goodrich and Bird* [1985].

Table 3. Carbon Isotope Data for This Study[a]

Area (Sample)	δ^{13}C Fe-Carbide	Area (Sample)	δ^{13}C Diamond	ΔC
Area D (Jag 5)		*Area D (Jag 5)*		
JAG5-D7-1	−20.1	JAG5-D2	−12.9	
JAG5-D7-2	−19.1	JAG5-D3	−13.5	
JAG5-D7-3	−19.2	-	-	
Area D mean	−19.5	Area D mean	−13.2	6.4
± δ in ‰ (1σ)	0.6	± δ in ‰ (2σ)	1.6	
Area F (Jag 5)		*Area F (Jag 5)*		
JAG5-F1	−16.9	JAG5-F1	−11.7	
JAG5-F2	−18.4	-	-	
JAG5-F3	−17.1	-	-	
JAG5-F4	−18.8	-	-	
JAG5-F6	−19.3	-	-	
Area F mean	−18.1	Area F	−11.7	6.5
± δ in ‰ (1σ)	1.1	± δ in ‰ (2σ)	1.5	
Area B (Jag10)		*Area B (Jag10)*		
AreaB4-1	−23.8	Area B4-1	−17.1	
AreaB4-2	−27.5	Area B4-2	−17.7	
AreaB4-3	−24.4	Area B4-3	−16.8	
-	-	Area B4-4	−17.2	
-	-	Area B4–5	−17.9	
-	-	Area B4–6	−17	
Area B mean	−25.2	Area B mean	−17.2	8.1
± δ in ‰ (1σ)	2	± δ in ‰ (2σ)	0.6	
			Average	7.2
			StDev	1.3

[a]Area F, D, and B simply reflect the names of target areas for isotopic analysis for each sample. Most areas of iron carbide identified using the NanoSIMS exhibited too much topography for reliable data acquisition.

produced during polishing with a diamond polishing scaife (T. Stachel, personal communication, 2013). This was investigated by laser sectioning samples Jag5 across the Fe-carbide to expose the interior of the polished plate to assess the depth of the Fe-carbide (supporting information Figure S4), which shows the Fe-carbide runs throughout the thickness of the polished plate (ca. 500 μm), thus confirming the Fe-carbide is not veneer deposited on the surface of the sample during polishing with a diamond polishing scaife, but is indeed native to the diamond.

The textures and phase relations for the Fe-carbide-diamond associations in these two samples differ considerably from previous documented occurrences of Fe-carbide in mantle diamonds. Fe-carbide from the 23rd Party Congress kimberlite, Russia [*Bulanova and Zayakina*, 1991] and Juina, Brazil [*Kaminsky and Wirth*, 2011] are associated with graphite and Fe-carbide spherules from Venieta, Botswana are found within garnet inclusions [*Jacob et al*., 2004]. Whereas the Fe-carbide in these samples is in solely contact with diamond and contains minor, but significant Si and O. The Fe-carbide is present as angular inclusions and also appears like an epigenetic crack-infill (Figures 2 and 3), but there are lines of evidence to suggest otherwise. The samples exhibit textures very similar to a synthetic diamond grown at high pressure and temperature using a Fe-Ni alloy solvent catalyst at 15–20 GPa and 2000–2100°C, therefore, the metallic infill is syngenetic with the diamond for the experimental sample (shown in Figure 3a). Unfortunately, the authors did not measure the composition of the Fe-Ni alloy prior to acid treatment [*Tomlinson et al*., 2011] and therefore we can only assume that they were Fe-Ni carbides based on the known phase equilibria in the system Fe-C [see *Lord et al*., 2009]. The contact between the Fe-carbide and the diamond in the samples presented here also forms rounded features, (Figure 3) and small ($<$0.5 μm^2) spherical "blebs" of Fe-carbide within the diamond host (Figure 4); both are difficult or impossible to explain by fracturing diamond. Because diamond is neither porous nor permeable and no cracks can be identified as feeder networks to these "blebs," we therefore find the best explanation for their existence to be liquid/melt immiscibility and therefore synchronous growth. Further evidence for syngeneic relations is octahedral inclusions within the diamond host (Figure 5). The octahedral morphology of these inclusions is not natural for Fe-carbides (typically orthorhombic). The octahedral morphology is imposed by the diamond host and therefore demonstrates syngenesis [*Meyer*, 1987]. Complimentary to textural observations are the near-constant difference for $\Delta C_{C\text{-}FeC}$ (within error) in the two samples where the individual diamond and Fe-carbide in the two samples exhibit differing δ^{13}C values outside of the analytical error (Table 3).

5.2. Isotopic Equilibrium?

Our data are in good agreement with the previous studies that show Fe-carbide to be ^{13}C-depleted relative to crystalline elemental carbon [*Deines and Wickman*, 1975; *Satish-Kumar et al*., 2011; *Reutsky et al*., 2012]. However, our mean $\Delta^{13}C$ of $+7.2 \pm 1.3‰$ is considerably smaller that what has been observed in the literature for graphite—Fe-carbide in Fe-meteorites [*Deines and Wickman*, 1975]. This may reflect a higher temperature and or higher pressure origin for our samples. Whether the carbon isotopes have reached isotopic equilibrium in this system is difficult to decipher with the available data because this is a two-stable isotope system. One may argue that a Fe-carbide containing Si and O is evidence of chemical disequilibrium that may also mean isotopic disequilibrium. A counter argument would be that between Fe-carbide and diamond one expects the Si and O to partition into the Fe-carbide. Because the samples exhibit differing $\delta^{13}C$ values but exhibit the same $\Delta C_{C\text{-}FeC}$ value (within error) we assume isotopic equilibrium has been achieved for these samples (Table 3).

5.3. Sample Petrogenesis

This is not the first report of Fe-carbide inclusions in mantle diamond from the Jagersfontein kimberlite [*Sharp*, 1966], nor as inclusions in mantle diamond [*Bulanova and Zayakina*, 1991; *Kaminsky and Wirth*, 2011] and garnet [*Jacob et al*., 2004]. Therefore, comparisons are possible where data permit. The Fe-carbide in this study has Ni contents that are below stoichiometric abundances for cohenite with $\leq$0.4 wt % Ni; however, the low Ni contents are comparable to the Fe-carbide from Disko Island, Greenland (Table 2). The atomic Fe/C ratio of these samples is distinct from one another, and also from any known natural iron carbides from the mantle. Jag5 has a Fe/C ratio of 3.25, which is close to what is observed at Disko Island, Greenland (2.91) [*Downs*, 2006] and cohenite from Venetia (2.90) [*Jacob et al*., 2004]. The atomic Fe/C ratio of the iron carbide in Jag10 is 4.31 (Table 2), which is not similar to any known carbide [*Oganov et al*., 2013]. The atomic Fe/C ratios for the iron carbides here are generally higher than those reported for a single diamond inclusion from Juina, Brazil, which exhibits a range from 1.66 to 3.33 [*Kaminsky and Wirth*, 2011]. Another feature, which makes these iron carbides distinct, are their bulk major element compositions. For example, Jag5 has 2.04 wt % Cr and 1.65 wt % Si, whereas Jag10 has 3.99 wt % O and 0.78 wt % Si [*Oganov et al*., 2013]. This can explain why their Fe/C ratios are not (a) like any known carbide or (b) comparable between these two samples. What these data highlight is the need for more complex, composite chemical phase diagrams for carbides in the deep Earth. For example, the stability and chemical composition of iron carbides in equilibrium with mantle minerals need to be quantified [*Oganov et al*., 2013]. The concentrations of Si and O within some regions of the carbide could be due to a variety of exsolved submicron-sized phases, suggesting minerals such as moissanite (SiC), fayalite ($FeSiO_4$), or possibly ferrosilite ($Fe_2Si_2O_6$). However, we cannot match any of these phases by stoichiometry using the data in Table 2. This could indicate that these elements (Cr, Ni, Si, O) were dissolved in a Fe^0 or Fe-carbide melts which is plausible, for example, Si and O are both soluble in Fe melts [*Takafuji et al*., 2005].

The fO_2 conditions that enabled Fe-carbide to precipitate cannot be calculated using the assemblage in this study, but we postulate that is below the IW buffer for two reasons; (1) above IW one would expect Fe oxides or Fe-rich ferromagnesian silicates [*Jacob et al*., 2004] and (2) the low Ni contents from 0.1 to 0.4 wt % (Table 1) can be explained by the fO_2 being below the IW buffer [*Rohrbach and Schmidt*, 2011]. Where the $\log fO_2$ is close to the IW buffer the native mantle Fe should be a Ni-rich alloy, but below the IW ($<$0 log units) the native Fe in the mantle should be almost pure Fe^0 [*Rohrbach and Schmidt*, 2011]. However we cannot rule out that the Fe^0 originated from subducted Ni-poor oceanic crust that reequilibrated with the mantle (akin to the model of *Jacob et al*. [2004]). Below we postulate the following working model that encompasses all of the observations presented above (note, that depth pressure and temperature cannot be defined due to a lack of available geochemical constraints):

1. The diamond was residing in a mantle domain where Fe^0 is stable, either $>$250 km [*Rohrbach et al*., 2007] or within an unusually reducing domain of cratonic lithosphere within the Kaapvaal Craton akin to the model of *Jacob et al*. [2004].

2. The diamond and liquid Fe^0 came into contact causing a reaction of $C^0 + Fe^0$ under mantle pressure and temperature conditions. This is not an equilibrium assemblage [*Lord et al*., 2009] and so the Fe^0 begins to react with C^0.

3. The first reaction was to dissolve carbon into the Fe^0 whilst infiltrating the diamond along slip/fracture planes (or other structural lines of weakness). The only phase present here are P-T dependant, but will

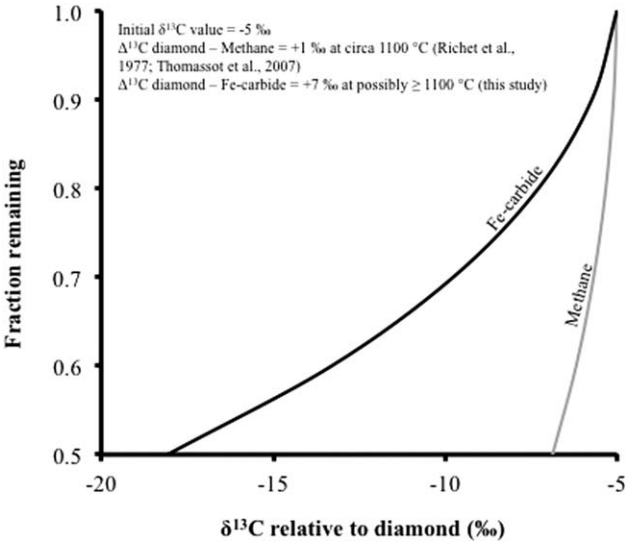

Figure 6. Calculated isotopic evolution of methane and Fe-carbide relative to diamond as a function of Rayleigh fractionation. The parameters for the calculations are shown in the figure, the initial δ^{13}C value is $-5‰$, the *y* axis shows fraction remaining, which is proportional to the fraction of diamond removed from an open-system (Rayleigh fractionation), the fraction removed is 0.1 per stage, and the fractionation factors (assuming temperature $=1200°$C) used are Δ^{13}C methane-diamond $=-1‰$ [*Bottinga*, 1969] and Δ^{13}C iron carbide-diamond $=-7‰$ (this study). The curve follows the evolution of the residual methand and Fe-carbide following the removal of diamond from the system.

most likely to be Fe-carbides in equilibrium with a melt (mix of Fe^0, dissolved C) until the carbon concentrations reaches above circa 6 wt % in the metal, at which point phase equilibria are expected to be diamond + Fe-carbide at >6 GPa and $>1100°$C [*Lord et al*., 2009].

4. The carbon-saturated metal precipitated Fe-carbide and reprecipitated diamond. This explains the sharp contact macroscopic textures in Figure 2, the similarity in textures for the synthetic sample grown in Fe-Ni alloy with the samples in this study (Figure 3a), the spherical blebs that resemble immiscible fluids in Figure 4, the Fe-carbide inclusions with an octahedral morphology (Figure 5), and the constant ΔC between the two phases (Table 3).

Our data imply that the reaction between $C^0 + Fe^0$ under mantle conditions can produce shifts in δ^{13}C of circa $7.2 \pm 1.3‰$. However, we do not have any temperature, pressure, or redox constrains for this empirical isotopic parameter. Below we explore the potential importance for the large Δ^{13}C presented here.

5.4. Broad Implications of These Data

At mantle depths $>\sim$250 km, fO_2 is buffered close to or below the IW buffer [*Frost et al*., 2004; *Rohrbach et al*., 2007]. Under these conditions, methane is the dominant carbonaceous fluid species in the deep Earth in equilibrium with diamond [*Blundy et al*., 1991]. The magnitude of isotopic fractionation for diamond-CH_4 is only circa $+1‰$ at 1200°C [*Bottinga*, 1969], as opposed to $-3.5‰$ for diamond-CO_2 at the same temperature (circa 1100°C) [*Richet et al*., 1977]. This lead *Stachel* [2001] to conclude that diamond formation in the sublithospheric mantle would produce minimal isotopic fractionation of ^{13}C due to the small Δ^{13}C of $<1‰$ for the reaction diamond-CH_4 at temperatures $>1100°$C (exemplified by the methane curve in Figure 6). However, as shown in Figure 1, the assemblage investigated here (diamond + Fe-carbide) is predicted in the deeper Earth [*Rohrbach and Schmidt*, 2011], and we have shown that this assemblage can generate a larger fractionation for the stable isotopes of carbon relative to diamond-CH_4 and diamond-CO_2. This demonstrates that isotopic fractionation in the deeper, more reducing mantle has the potential to produce ^{13}C-depleted and ^{13}C-enriched reservoirs by a mantle-derived (abiogenic) reaction (Figure 6). Although ^{13}C-enriched diamonds are extremely uncommon, a considerable proportion of transition zone samples do show ^{13}C-enrichment, therefore such a potential reaction should not be discounted outright. For example, reported δ^{13}C values of diamond samples interpreted to have been derived from the transition zone exhibit carbon isotope modes for δ^{13}C at $\sim-8‰$ (Juina, Brazil) [*Hutchison et al*., 1999]; $\sim+1‰$ (Kankan, West African) [*Palot et al*., 2012], and $-19‰$, (Jagersfontein, S. Africa) [*Deines et al*., 1991].

It is noteworthy that, if the deep mantle contains $\sim$1 wt % Fe^0 [*Frost et al*., 2004; *Rohrbach et al*., 2007], then so long as the carbon content in the Fe^0 is <6 wt %, we expect only Fe-carbide to be present. In addition, with a high fH_2 then there exists a possibility for Fe-carbide + methane as the dual speciation of carbon, however, the stable isotope fractionation factors in this system are unknown. Consequently, the data presented here have important implications. First, diamond formation involving Fe-carbide in the deeper, hotter and more reducing mantle may also result in larger fractionation of $^{13}C/^{12}C$ relative to the shallower, more oxidizing and colder mantle. Second, large-scale, measurable carbon isotope fractionation during

carbon partitioning into the metallic phase during core formation now appears very likely (as postulated by *Wood et al*. [2013]). Finally, these data also demonstrate the effect of Cr-Si-O abundances in the Fe-carbide do not have a resolvable effect on the partitioning of $^{13}C/^{12}C$ between Fe-carbide and diamond.

6. Concluding Remarks

We conclude that the samples in this study formed by interaction between mantle diamond and native iron, but we cannot ascertain whether this occurred in the upper, transitional, or lower mantle. Similarly, we cannot ascertain whether the carbon and/or iron came from the ambient mantle or from a subducted source. The diamond and iron reacted to precipitate diamond and iron-carbide that resulted in partitioning of ^{13}C between the two phases. This study demonstrates that isotopic fractionation of $^{13}C/^{12}C$ of up to $\sim>7‰$ can occur in the mantle at minimum temperatures and pressures consistent with the top of the diamond stability field. We interpret formation conditions to have been reducing, with fO_2 at or below the iron-iron wustite redox buffer in a cratonic or deep mantle environment in Earth. The cogenesis of carbide and diamond may produce abiogenic reservoirs of ^{13}C-depleted carbon that overlap isotopically "light" carbon conventionally attributed to subducted organic carbon. Finally, the large $\Delta^{13}C$ for diamond-iron carbide observed here implies that determination of the $\Delta^{13}C$ for silicate-metallic melts might be used to constrain future estimates of the distribution of carbon between the Earth's metallic core and silicate mantle.

Acknowledgments

S.M. would like to thank the Engineering and Physical Sciences Research Council, the Diamond Trading Company, and the Department of Physical Sciences, The Open University (UK) for financial support during his time as a PhD student at University College London (UK). The Geophysical Laboratory, Carnegie Institution of Washington is also acknowledged through the award of a Carnegie postdoctoral fellowship to S.M. where this work was completed. Bulk carbon isotopic measurements were performed by M. A. Gilmour, PSS, Open University, UK. NanoSIMS work was possible, thanks to STFC support for UKCAN. We are grateful for constructive and critical reviews from Pierre Cartigny, Emilie Thomassot, Thomas Stachel, Dorrit Jacob, Felix Kaminsky, and an anonymous reviewer, and the editorial handling of Janne Blichert-Toft and Paul Asimow greatly improved the quality of this manuscript.

References

Blundy, J. D., J. P. Brodholt, and B. J. Wood (1991), Carbon fluid equilibria and the oxidation-state of the upper mantle, *Nature*, *349*, 321–324.

Bottinga, Y. (1969), Calculated fractionation factors for carbon and hydrogen isotope exchange in the system calcite-carbon dioxide-graphite-methane-hydrogen-water vapor, *Geochim. Cosmochim. Acta*, *33*, 49–64.

Boyd, S. R., and C. T. Pillinger (1994), A preliminary study of $^{15}N/^{14}N$ in octahedral growth form diamonds, *Chem. Geol.*, *116*, 43–59.

Bulanova, G. P., and N. V. Zayakina (1991), Graphite–iron–cohenite assemblage in the central zone of diamond from 23rd Party Congress kimberlite [in Russian], *Dokl. Akad. Nauk SSSR*, *317*, 706–709.

Deines, P. (2002), The carbon isotope geochemistry of mantle xenoliths, *Earth Sci. Rev.*, *58*, 247–278.

Deines, P., and F. E. Wickman (1975), A contribution to the stable carbon isotope geochemistry of iron meteorites, *Geochim. Cosmochim. Acta*, *39*, 547–557.

Deines, P., J. W. Harris, and J. J. Gurney (1991), The carbon isotopic composition and nitrogen content of lithospheric and asthenospheric diamonds from the Jagersfontein and Koffiefontein kimberlite, South Africa, *Geochim. Cosmochim. Acta*, *55*, 2615–2625.

Di Pierro, S., E. Gnos, B. H. Grobety, T. Armbruster, S. M. Bernasconi, and P. Ulmer (2003), Rock-forming moissanite (natural α-silicon carbide), *Am. Mineral.*, *88*, 1817–1821.

Downs, R. T. (2006), The RRUFF project: An integrated study of the chemistry, crystallography, Raman and infrared spectroscopy of minerals, paper presented at 19th General Meeting of the International Mineralogical Association [Program and Abstracts], Kobe, Japan.

Fitzsimons, I. C. W., B. Harte, and R. M. Clark (2000), SIMS stable isotope measurement: Counting statistics and analytical precision, *Mineral. Mag.*, *64*, 59–83.

Frost, D. J., C. Liebske, F. Langenhorst, C. A. McCammon, R. G. Tronnes, and D. C. Rubie (2004), Experimental evidence for the existence of iron-rich metal in the Earth's lower mantle, *Nature*, *428*, 409–412.

Goodrich, C. A., and J. M. Bird (1985), Formation of iron-carbon alloys in basaltic magma at Uivfaq, Disko Island: The role of carbon in mafic magmas, *J. Geol.*, *93*, 475–492.

Hutchison M.T., Cartigny P., Harris J.W. (1999), Carbon and nitrogen compositions and physical characteristics of transition zone and lower mantle diamonds from Sao Luiz, *Brazil. Proc. Int. Kimberlite Conf.*, 7th *7*, 372–382.

Jacob, D. E., A. Kronz, and K. S. Viljoen (2004), Cohenite, native iron and troilite inclusions in garnets from polycrystalline diamond aggregates, *Contrib. Mineral. Petrol.*, *146*, 566–576.

Jones, A. P., D. P. Dobson, I. Wood, A. D. Beard, A. B. Verchovsky, and H. J. Milledge (2008), Iron carbide and metallic inclusions in diamonds from Jagersfontein, abstract 9IKC-A-00360 presented at Ninth International Kimberlite Conference, Frankfurt, Germany.

Kaminsky, F. V., and R. Wirth (2011), Iron carbide incluisons in lower-mantle diamond from Juina, Brazil, *Can. Mineral.*, *49*, 555–572.

Leung, I., W. Guo, I. Friedman, and J. Gleason (1990), Natural occurrence of silicon carbide in a diamondiferous kimberlite from Fuxian, *Nature*, *346*, 352–354.

Lord, O. T., M. J. Walter, R. Dasgupta, D. Walker, and S. M. Clark (2009), Melting in the Fe-C system to 70 GPa, *Earth Planet. Sci. Lett.*, *284*, 157–167.

Mathez, E. A., R. A. Fogel, I. D. Hutcheon, and V. K. Marshintsev (1995), Carbon isotopic composition and origin of SiC from kimberlites of Yakutia, Russia, *Geochim. Cosmochim. Acta*, *59*, 781–791.

Meyer, H. O. A. (1987), Inclusions in diamond, in *Mantle Xenoliths*, edited by P. H. Nixon, pp. 501–522, John Wiley, Chichester, U.K.

Oganov, A. R., R. J. Hemley, R. M. Hazen, and A. P. Jones (2013), Structure, bonding, and mineralogy of carbon at extreme conditions, in Carbon in Earth, edited by R. M. Hazen, A. P. Jones, and J. Baross, *Rev. Mineral. Geochem.*, *75*, 47–77.

Palot, M., P. Cartigny, J. W. Harris, F. V. Kaminsky, and T. Stachel (2012), Evidence for deep mantle convection and primordial heterogeneity from nitrogen and carbon stable isotopes in diamond, *Earth Planet. Sci. Lett.*, *357*–358, 179–193.

Papineau, D., B. T., De Gregorio, R. M. Stroud, A. Steele, E. Pecoits, K. Konhauser, J. Wang, M. L. Fogel, (2010), Ancient graphite in the Eoarchean quartz-pyroxene rocks from Akilia in southern West Greenland II: Isotopic and chemical compositions and comparison with Paleoproterozoic banded iron formations, *Geochimica Et Cosmochimica Acta 74*, 5884–5905.

Reutsky, V. N., M. Borzdov, and N. Palyanov (2012), Effect of diamond growth rate on carbon isotope fractionation in Fe–Ni–C system, *Diamond Related Mater.*, *21*, 7–10.

Reutsky, V. N., and Yu. M. Borzdov (2013), A comment on "Experimental determination of carbon isotope fractionation between iron carbide melt and carbon: 12C-enriched carbon in the Earth's core?" by M. Satish-Kumar, H. So, T. Yoshino, M. Kato, Y. Hiroi [Earth Planet. Sci. Lett. 310 (2011) 340–348], *Earth Planet. Sci. Lett.*, *368*, 219–221.

Richet, P., Y. Bottinga, and M. Javoy (1977), A review of hydrogen, carbon, nitrogen, oxygen, sulphur, and chlorine stable isotope fractionation among gaseous molecules, *Annu. Rev. Earth Planet. Sci.*, *5*, 65–110.

Rohrbach, A., and M. W. Schmidt (2011), Redox freezing and melting in the Earth's deep mantle resulting from carbon-iron redox coupling, *Nature*, *472*, 209–212.

Rohrbach, A., C. Ballhaus, U. Golla-Schindler, P. Ulmer, V. S. Kamenetsky, and D. V. Kuzmin (2007), Metal saturation in the upper mantle, *Nature*, *449*, 456–458.

Satish-Kumar, M., H. So, T. Yoshino, M. Kato, and Y. Hiroi (2011), Experimental determination of carbon isotope fractionation between iron carbide melt and carbon: ^{12}C-enriched carbon in the Earth's core?, *Earth Planet. Sci. Lett.*, *310*, 340–348.

Satish-Kumar, M., H. So, T. Yoshino, M. Kato, and Y. Hiroi (2013), Reply to comment by Reutsky and Borzdov on "Carbon isotope fractionation in the system Fe-C at HPHT experiments," *Earth Planet. Sci. Lett.*, *368*, 222–224.

Sharp, W. E. (1966), Pyrrhotite: A common inclusion in South African diamonds, *Nature*, *211*, 402–403.

Shirey, S. B., P. Cartigny, D. J. Frost, S. Keshav, F. Nestola, P. Nimis, D. G. Pearson, N. V. Sobolev, and M. J. Walter (2013), Diamonds and the Geology of mantle carbon, in Carbon in Earth, edited by R. M. Hazen, A. P. Jones, and J. Baross, *Rev. Mineral. Geochem.*, *75*, 355–421.

Stachel, T. (2001), Diamonds from the asthenosphere and the transition zone, *Eur. J. Mineral.*, *13*, 883–892.

Takafuji, N., K. Hirose, M. Mitome, and Y. Bando (2005), Solubilities of O and Si in liquid iron in equilibrium with (Mg,Fe)SiO_3 perovskite and the light elements in the core, *Geophys. Res. Lett.*, *32*, L06313, doi:10.1029/2005GL022773.

Tappert, R., T. Stachel, J. W. Harris, K. Muehlenbachs, T. Ludwig, and G. P. Brey (2005), Subducting oceanic crust: The source of deep diamonds, *Geology*, *33*, 565–568.

Thomassot, E., P. Cartigny, J. W. Harris, and K. S. F. Viljoen (2007), Methane-related diamond crystallization in the Earth's mantle: Stable isotope evidences from a single diamond-bearing xenolith, *Earth Planet. Sci. Lett.*, *257*, 362–371.

Tomlinson, E. L., D. Howell, A. P. Jones, and D. J. Frost (2011), Characteristics of HPHT diamond grown at sub-lithosphere conditions (10–20 GPa), *Diamond Related Mater.*, *20*, 11–17.

Wallace, P. J. (2005), Volatiles in subduction zone magmas: concentrations and fluxes based on melt inclusion and volcanic gas data, *J. Volcanol. Geotherm. Res.*, *140*, 217–240.

Wood, B. J., J. Li, and A. Shahar (2013), Carbon in the core: Its influence on the properties of core and mantle, *Rev. Mineral. Geochem.*, *75*, 231–250.